Title:
Regulation of sugar transporter activity for antibacterial defense in *Arabidopsis*

Authors:
Kohji Yamada[1,2,*], Yusuke Saijo[3,4], Hirofumi Nakagami[5†], Yoshitaka Takano[1,*]

Affiliations:

[1] Graduate School of Agriculture, Kyoto University, Kyoto, Japan.

[2] Graduate School of Bioscience and Bioindustry, Tokushima University, Tokushima, Japan.

[3] Graduate School of Biological Sciences, Nara Institute of Science and Technology, Ikoma, Japan.

[4] JST, PRESTO, Kawaguchi, Japan.
[5] RIKEN Center for Sustainable Resource Science, Yokohama, Japan.

[†] Current address: Max Planck Institute for Plant Breeding Research, Cologne, Germany.

[*]Corresponding author. Email: kohjiyamada226@gmail.com (K.Y.); ytakano@kais.kyoto-u.ac.jp (Y.T.)

Abstract:

Microbial pathogens strategically acquire metabolites from their hosts during infection. Here we show that the host can intervene to prevent such metabolite loss to pathogens. Phosphorylation-dependent regulation of sugar transport protein 13 (STP13) is required for antibacterial defense in the plant *Arabidopsis thaliana*. STP13 physically associates with the flagellin receptor flagellin-sensitive 2 (FLS2) and its co-receptor BRASSINOSTEROID INSENSITIVE 1-associated receptor kinase 1 (BAK1). BAK1 phosphorylates STP13 at threonine 485, which enhances its monosaccharide uptake activity to compete with bacteria for extracellular sugars. Limiting the availability of extracellular sugar deprives bacteria of an energy source and restricts virulence factor delivery. Our results reveal that control of sugar uptake, managed by regulation of a host sugar transporter, is a defense strategy deployed against microbial infection. Competition for sugar thus shapes host-pathogen interactions.

One sentence summary:
Phosphorylation of the sugar transporter STP13 promotes *Arabidopsis* sugar uptake in competition with pathogens for extracellular sugars

Short title:
Sugar transporter regulation in plant defense

Main text:

Plants assimilate carbon into sugar by photosynthesis, and a broad spectrum of plant-interacting microbes exploits these host sugars (*1, 2*). In *Arabidopsis*, pathogenic bacterial infection causes the leakage of sugars to the extracellular spaces (the apoplast) (*3*), a major site of colonization by plant-infecting bacteria. While leakage may be a consequence of membrane disintegration during pathogen infection, some bacterial pathogens promote sugar efflux to the apoplast by manipulating host plant sugar transporters (*4, 5*). Interference with sugar absorption by bacterial and fungal pathogens reduces their virulence, highlighting a general importance of sugar acquisition for microbial infection (*4-7*).

Plants control apoplastic sugar levels by sugar transporters and glycoside hydrolases. For example, sucrose exported to the apoplast is hydrolyzed to glucose and fructose by cell wall-bound invertases (cwINVs), which are then transported to the cytoplasm by sugar transport proteins (STPs) (*8*). Of the 14 *Arabidopsis* STP transporters, STP1 and STP13 largely govern the uptake of monosaccharides (*9*). In plant defense, STP13 contributes to resistance against the gray mold fungus *Botrytis cinerea* in *Arabidopsis* (*10*). On the contrary, the *Lr67res* mutation, which results in impaired transporter activity of LR67 (an STP13 ortholog), enhances resistance against both rust and powdery mildew fungal pathogens in wheat although the process remains undetermined (*11*).

Here, to investigate whether sugar uptake by STP1 and STP13 contributes to antibacterial defense in *Arabidopsis*, we spray-inoculated the phytopathogenic bacterium *Pseudomonas syringae* pv. *tomato* (*Pst*) DC3000 (*12*) onto *stp1 stp13* double mutant plants. The plants showed increased susceptibility to *Pst* DC3000 (Fig. 1A left), but exhibited a wild-type (WT)-like stomatal closure response (*13*) to the flg22 peptide of bacterial flagellin (fig. S1). Thus, the elevated susceptibility of *stp1 stp13* plants seems to reflect defects in their post-invasion defenses. Indeed, growth of syringe-infiltrated *Pst* DC3000 *ΔhrcC*, a less virulent strain lacking the type III secretion system (T3SS) that delivers virulence factors called effectors into plant cells, was also elevated in *stp1 stp13* plants (Fig. 1A right). Our results suggest that STP1 and STP13 restrict bacterial proliferation in the apoplast by retrieving sugars.

To determine whether apoplastic monosaccharide levels fluctuate during antibacterial defense, we measured apoplastic glucose levels following exposure to flg22. Apoplastic glucose levels in the leaves of *stp1 stp13* plants were significantly higher than in WT plants, but were indistinguishable from WT in non-elicited plants (fig. S2A). Moreover, cwINV activity was comparably induced in WT and *stp1 stp13* plants in response to flg22 (fig. S2B). Together, these data indicate that STP1 and/or STP13 absorb cwINV-generated monosaccharides in the apoplast during antibacterial defense, and thus perhaps significantly reduce apoplastic sugar content during bacterial challenge.

We also found that monosaccharide uptake activity in *Arabidopsis* seedlings increased after flg22 application, but not in the absence of the leucine-rich repeat receptor kinase (LRR-RK) FLS2, the flg22 receptor in *Arabidopsis* (Fig. 1B), further suggesting that plants actively absorb sugars during antibacterial defense. Because the contribution of STP1 and STP13 to

antibacterial defense implies their roles in flg22-induced monosaccharide uptake activity in *Arabidopsis* plants, we measured monosaccharide uptake in *stp1* and *stp13* plants upon mock and flg22 application. *stp1* plants retained an increase in monosaccharide uptake in response to flg22 while the basal activity of mock-treated plants was reduced (Fig. 1B). In contrast, *stp13* plants failed to show enhanced activity after flg22 application (Fig. 1B). This demonstrated that STP1 and STP13 contribute to basal and flg22-induced monosaccharide uptake activity, respectively. Consistent with this role of STP13, the introduction of functional STP13-GFP (*9*) expressed by native *STP13* regulatory DNA sequences eliminated the elevated apoplastic glucose levels of *stp1 stp13* plants in response to flg22 (fig. S2C). Nevertheless, STP1 and STP13 seem to work redundantly in antibacterial defense, given the enhanced susceptibility of *stp1 stp13* double mutants, but not *stp13* single mutants, to *Pst* DC3000 (Fig. 1A left). STP1-mediated activity may compensate for the absence of STP13 by absorbing monosaccharide beyond the threshold required for bacterial suppression. Indeed, simultaneous loss of STP1 and STP13 caused significantly lowered monosaccharide uptake with or without flg22 application (Fig. 1B), which probably led to the enhanced susceptibility of *stp1 stp13* plants.

The STP13 dependence of flg22-induced monosaccharide uptake prompted us to explore the molecular mechanisms for regulation of STP13 activity during antibacterial defense. We found that *STP13* but not *STP1* expression was induced in response to flg22 (fig. S3). STP13-GFP protein level also rose in seedlings and mature leaves following flg22 application (Fig. 1C and fig. S4). STP13-GFP fluorescence spread at the plasma membranes of epidermal and mesophyll cells after flg22 application, but was detected mainly to guard cells upon mock treatment (Fig. 1D). Thus, *STP13* was transcriptionally activated during antibacterial defense.

Post-translational modifications including phosphorylation can also modulate transporter activity (*14*), and to investigate such modification of STP13 during antibacterial defense, we first identified STP13-interacting proteins. The initiation of plant immunity occurs when exogenous or endogenous immune elicitors are perceived by pattern-recognition receptors (PRRs) at the plasma membrane (*15*), where STP13 is also localized. We tested whether STP13 associates with PRRs by co-immunoprecipitation (co-IP) analysis, using a transient expression system in *Nicotiana benthamiana*. STP13-FLAG co-immunoprecipitated with GFP fusions of FLS2 and two other PRRs, elongation factor-Tu receptor (EFR) and Pep receptor 1 (PEPR1), which recognize the elf18 peptide of bacterial elongation factor-Tu and the endogenous elicitor-active Pep peptides, respectively (*15, 16*) (fig. S5), but did not co-immunoprecipitate with the GFP fusion of the plasma membrane marker protein low temperature-inducible 6b (LTI6b) (fig. S5), indicating the specificity of STP13 interactions with these PRRs at the plasma membrane. Upon ligand perception, these PRRs associate with another LRR-RK, BAK1, which triggers the activation of downstream factors including the receptor-like cytoplasmic kinase botrytis-induced kinase 1 (BIK1) through *trans*-phosphorylation events (*15*). We found that BAK1-HA, as well as FLS2-HA, associated with STP13-FLAG in *Arabidopsis* protoplasts while BIK1-HA did not (Fig. 2A). Moreover, STP13-GFP associated with FLS2 and BAK1 in mock-treated and 10-h flg22-treated stable transgenic plants (Fig. 2B and fig S6); an FLS2-BAK1 association was also

detectable 10 h after flg22 application (fig. S7). From these interaction data, we infer that STP13 exists in complexes with FLS2 and/or BAK1, irrespective of their ligand-dependent activation states. The results suggest that STP13 participates in various PRR complexes, each of which may directly regulate STP13 activity during antibacterial defense.

We next asked whether STP13 is phosphorylated by PRR complexes *in vitro*. In multipass transmembrane proteins such as transporters, the longer cytoplasmic regions tend to be phosphorylated (*17*). We tested whether two STP13 fragments, the middle loop (ML, located between the 6th and 7th transmembrane domains) and the C-terminal tail (CT), expressed as glutathione S-transferase (GST) fusions in *Escherichia coli* could be phosphorylated (fig. S8A, S8B). A maltose binding protein (MBP) fusion to BAK1 cytoplasmic kinase domain (CD) phosphorylated GST-STP13 CT, but not GST-STP13 ML. Neither MBP-PEPR1 CD nor MBP-BIK1 phosphorylated STP13 fragments *in vitro* (fig. S8C). We used PEPR1 CD for this assay because FLS2 CD shows weak *in vitro* kinase activity (*18*). Several serine and threonine residues occur in the STP13 CT fragment (Fig. 2C top), including the previously reported phosphorylation site S513 (*17*). Although we substituted S513 with a non-phosphorylatable alanine (A) residue, MBP-BAK1 CD still phosphorylated GST-STP13 CT (S513A) (Fig. 2C left). On the other hand, BAK1-mediated STP13 phosphorylation was reduced by alanine substitution at T485 but unaffected by alanine substitutions at S517, S523 and T524 (Fig. 2C). We concluded that BAK1 phosphorylates STP13 at T485. The corresponding residue was conserved in STP13 orthologs of other plant species (fig. S9A), but rarely among *Arabidopsis* STP homologs (fig. S9B), implying that critical and specific regulation of STP13 occurs through T485 phosphorylation in plants.

To examine whether T485 phosphorylation affects the transporter activity of STP13, we tested the function of STP13 (T485D)-GFP, in which T485 was substituted with a phospho-mimic aspartic acid (D) residue. When introduced to a yeast strain deficient in multiple monosaccharide transporters, STP13 (T485D)-GFP promoted yeast growth on 10 mM glucose, more so than did STP13-GFP, although this enhancement became less clear at lower glucose concentrations (fig. S10A and S10B). In addition, STP13 (T485D)-GFP yeast cells absorbed more ^{14}C-labeled monosaccharides than STP13-GFP cells (Fig. 3A, fig. S10C). On the other hand, the T485A substitution did not affect monosaccharide uptake activity (Fig. 3A), indicating that basal sugar transport activity of STP13 is insensitive to the T485A substitution. Protein accumulation and intracellular localization of STP13 were unaffected by the T485D substitution (fig. S10D and S10E), which suggests that it affects STP13 transporter activity *per se*. We observed a low affinity (K_m value, 121.3 ± 6.3 μM) and high capacity (V_{max} value, 8.5 ± 0.6 nmol/10 min) of STP13 (T485D)-GFP cells for glucose, compared with a K_m of 71.7 ± 3.6 μM and a V_{max} of 3.3 ± 0.3 nmol/10 min of STP13 (T485A)-GFP cells (fig. S10F).

To test whether T485 phosphorylation also affects STP13 activity *in planta*, we measured flg22-induced glucose uptake in STP13-GFP and STP13 (T485A)-GFP plants in the *stp1 stp13* background. Although the T485A substitution did not affect STP13 activity in yeast cells or in non-elicited plants (Fig. 3A, 3B), it reduced flg22-induced glucose uptake activity in

plants (Fig. 3B). Protein accumulation in STP13-GFP and STP13 (T485A)-GFP plants was comparable (fig. S11). We concluded that STP13 underwent phosphorylation at T485 in response to flg22, which enhanced its sugar transport capacity. Glucose uptake in response to flg22 also increased somewhat in STP13 (T485A)-GFP plants (Fig. 3B), probably via transcriptional induction. Thus, STP13 activity is regulated at transcriptional and post-translational levels during antibacterial defense.

We investigated the contribution of STP13 T485 phosphorylation to antibacterial defense. Complementation of *stp1 stp13* mutant plants with STP13-GFP restored resistance to bacterial infection to WT levels (Fig. 3C), whereas the alanine-substituted version, STP13 (T485A)-GFP, was ineffective. Thus, regulation of STP13 activity through T485 phosphorylation is required for the plant to suppress bacterial proliferation.

Pathogens coordinate virulence factor expression in response to localized environments in their hosts. In the case of phytopathogenic bacteria such as *Pst* DC3000, T3SS regulatory cascades are activated via recognition of external sugars (*19*, *20*). We speculated that reduced sugar uptake activity in *stp1 stp13* plants might therefore augment bacterial effector delivery into plant cells. To test this, we inoculated plants with bacteria expressing the T3SS effector avrPto fused to adenylate cyclase (Cya) (*21*), which produces cAMP only when delivered into eukaryotic cells. We observed higher cAMP levels in *stp1 stp13* plants than in WT plants, without increased bacterial growth (Fig. 3D and fig. S12), indicating elevated effector delivery in *stp1 stp13* plants. Introduction of STP13-GFP, but not STP13 (T485A)-GFP, reversed this trend (Fig. 3D). We conclude that phosphorylation-dependent regulation of STP13 activity suppresses bacterial effector delivery. The likely mechanism is that STP13 reduces sugar content in the apoplast, resulting in limited bacterial T3SS activation.

Our findings illuminate a critical role for sugar transporter regulation during bacterial challenge (fig. S13). Stimulation of STP13 activity suppresses bacterial effector delivery (Fig. 3D), thereby reducing bacterial virulence. Moreover, the elevated growth of *ΔhrcC* strain, which is defective in T3SS effector delivery, in the apoplast of *stp1 stp13* plants (Fig. 1A right) suggests that apoplastic sugars represent an energy source for bacterial proliferation. Phytopathogenic bacteria exploit various host-derived metabolites, in addition to sugars, as energy sources or signaling molecules (*22*, *23*). Regulation of metabolite uptake upon recognition of microbial molecules may thus emerge as a key host defense strategy to restrict pathogen proliferation.

References and Notes:

1 R. T. Voegele, K. W. Mendgen, *Euphytica* **179**, 41-55 (2011).

2 J. Doidy et al., *Trends Plant Sci.* **17**, 413-422 (2012).

3 K. Wang, M. Senthil-Kumar, C. M. Ryu, L. Kang, K. S. Mysore, *Plant Physiol.* **158**, 1789-1802 (2012).

4 L. Q. Chen et al., *Nature* **468**, 527-532 (2010).

5 M. Cohn et al., *Mol. Plant Microbe Interact.* **27**, 1186-1198 (2014).

6 R. Wahl, K. Wippel, S. Goos, L. Kämper, N. Sauer, *PLoS Biol.* **8** (doi:10.1371/journal.pbio.1000303) (2010).
7 T. Li, B. Liu, M. H. Spalding, D. P. Weeks, B. Yang, *Nat. Biotechnol.* **30**, 390-392 (2012).
8 J. S. Eom et al., *Curr. Opin. Plant Biol.* **25**, 53-62 (2015).
9 K. Yamada et al., *J. Biol. Chem.* **286**, 43577-43586 (2011).
10 P. Lemonnier et al., *Plant Mol. Biol.* **85**, 473-484 (2014).
11 J. W. Moore et al., *Nat. Genet.* **47**, 1494-1498 (2015).
12 X. Y. Xin, S. Y. He, *Annu. Rev. Phytopathol.* **51**, 473-498 (2013).
13 W. Zeng, S. Y. He, *Plant Physiol.* **153**, 1188-1198 (2010).
14 K. H. Liu, Y. F. Tsay, *EMBO J.* **22**, 1005-13 (2003).
15 D. Couto, C. Zipfel, *Nat. Rev. Immunol.* **16**, 537-552 (2016).
16 K. Yamada et al., *EMBO J.* **35**, 46-61 (2016).
17 T. S. Nuhse, A. Stensballe, O. N. Jensen, S. C. Peck, *Plant Cell* **16**, 2394-2405 (2004).
18 B. Schwessinger et al., *PLoS Genet.* **7** (doi: 10.1371/journal.pgen.1002046) (2011).
19 T. V. Huynh, D. Dahlbeck, B. J. Staskawicz, *Science* **245**, 1374-1377 (1989).
20 J. L. Stauber, E. Loginicheva, L. M. Schechter, *Res. Microbiol.* **163**, 531-539 (2012).
21 L. M. Schechter, K. A. Roberts, Y. Jamir, J. R. Alfano, A. Collmer, *J. Bacteriol.* **186**, 543-555 (2004).
22 A. Rico, G. M. Preston, *Mol. Plant Microbe Interact.* **21**, 269-282 (2008).
23 J. C. Anderson et al., *Proc. Natl. Acad. Sci. U.S.A.* **111**, 6846-6851 (2014).

Acknowledgements:
We thank Dr. Suthitar Singkaravanit-Ogawa and Mr. Taishi Hirase for technical support, and Dr. Ian Smith for critical reading. We thank Drs. Kazuko Yamaguchi-Shinozaki, Seiji Tsuge, John M. Ward, Anke Reinders and Junro Mogami for published materials. This work was supported by JSPS KAKENHI (14J04880 and 16K18656, K.Y.; 15H01247, H.N.; 15H04457 and 15H05780, Y.T.), by JST PRESTO (Y.S.) and by the Asahi Glass Foundation (Y.T.). K.Y. and Y.T. conceived this study. K.Y. performed all experiments and data analyses. H.N. provided technical assistance. K.Y., Y.S. and Y.T. designed experiments and wrote the manuscript. Supplement contains additional data.

Supplementary materials:
Materials and Methods
Figs. S1 to S13
Table S1
References (*24-33*)

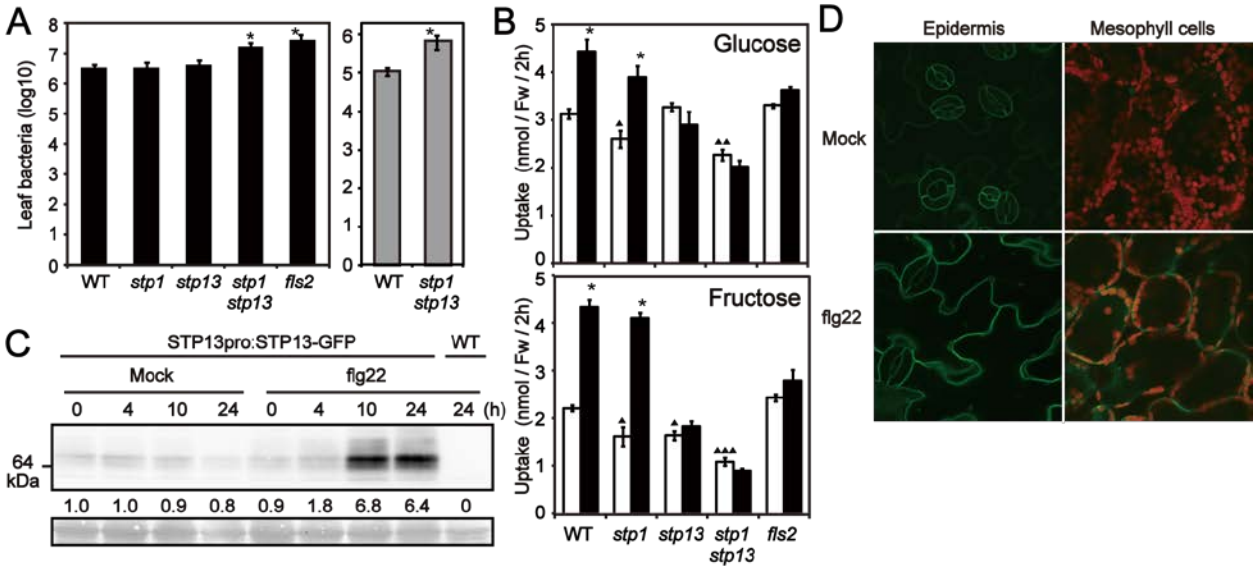

Fig. 1. Sugar transporters STP1 and STP13 contribute to antibacterial defense, and STP13 activity is induced in response to flg22. (A) Growth of spray-inoculated *Pst* DC3000 (black) or syringe-inoculated *Pst* DC3000 *ΔhrcC* (gray) in *Arabidopsis* leaves. Results are averages ± SE, $n = 5$ (*, $p < 0.05$ compared to the corresponding values of WT plants in two-tailed *t*-tests). **(B)** ^{14}C-labeled monosaccharide uptake activity in *Arabidopsis* seedlings 24 h after water (mock, white) or 4 µM flg22 (black) application. Results are averages ± SE, $n = 3$ (*, $p < 0.05$ compared to the corresponding values of each mock treatment; ▲, $p < 0.05$, ▲▲, $p < 0.005$, ▲▲▲, $p < 0.0005$ compared to the corresponding values of mock-treated WT plants; two-tailed *t*-tests). Fw, fresh weight of seedlings. **(C)** Anti-GFP immunoblot analysis for STP13-GFP in *Arabidopsis* seedlings exposed to water (mock) or 0.5 µM flg22. Numbers below the immunoblot represent relative intensities of STP13-GFP bands, normalized to backgrounds in Ponceau S-stained loading controls (bottom) and with the 0-h mock treatment value set as 1.0. **(D)** GFP fluorescence of STP13-GFP in *Arabidopsis* seedlings exposed to water (mock) or 0.5 µM flg22 for 10 h. Red fluorescence indicates autofluorescence of chloroplasts.

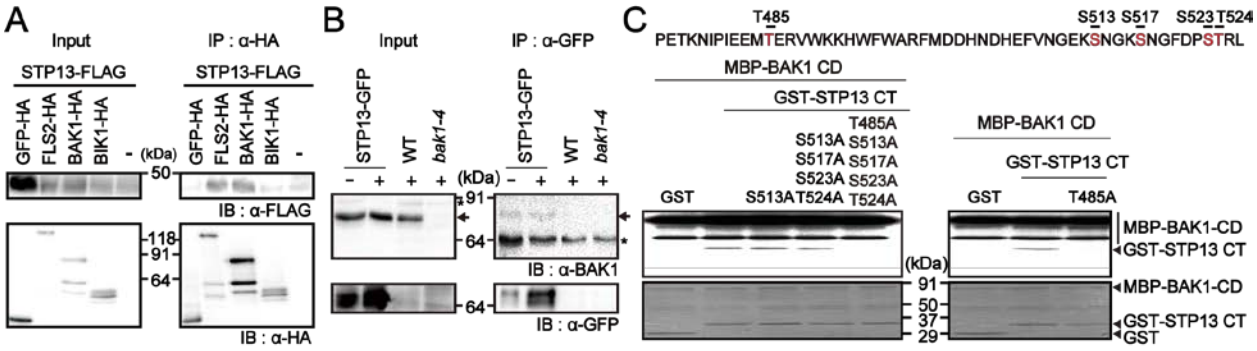

Fig. 2. STP13 participates in FLS2 complexes and is phosphorylated by BAK1. (A and B) Co-immunoprecipitation analysis between STP13 and known FLS2 complex components in *Arabidopsis* protoplasts (A) and transgenic *Arabidopsis* plants (B). + and - indicate 0.5 µM flg22 and mock treatment, respectively, for 10 h. IP and IB denote immunoprecipitation and immunoblotting with the indicated antibodies. BAK1 (arrows) and cross-reactive bands (asterisks) are indicated. **(C)** Autoradiograph of an *in vitro* kinase assay. Serine and threonine residues in the STP13-CT fragment (top) are highlighted in red. Coomassie Brilliant Blue-stained controls are shown below.

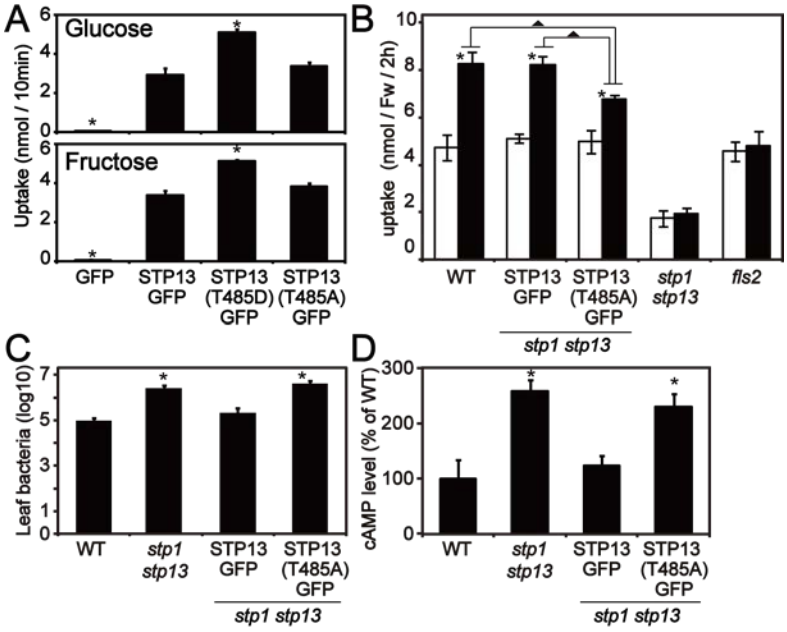

Fig. 3. Regulation of STP13 activity by T485 phosphorylation is required to suppress bacterial proliferation, partly by limiting virulence factor delivery. (A) ^{14}C-labeled monosaccharide uptake assay in yeast cells. Results are averages ± SE, $n = 3$ (*, $p < 0.05$ in two-tailed *t*-tests compared to the corresponding values of STP13-GFP cells). **(B)** Glucose uptake activity in *Arabidopsis* seedlings 24 h after water (mock, white) or 4 µM flg22 (black) application. Results are averages ± SE, $n = 3$ (*, $p < 0.05$, compared to the corresponding values of each mock treatment; ▲, $p < 0.05$, compared between indicated values; two-tailed *t*-tests). **(C)** Growth of spray-inoculated *Pst* DC3000 in *Arabidopsis* leaves. Results are averages ± SE, $n = 5$ (*, $p < 0.05$ compared to the values of WT plants using two-tailed *t*-tests). **(D)** cAMP amounts in *Arabidopsis* leaves at 10 h after spray inoculation with *Pst* DC3000 (avrPto-Cya). Results are averages ± SE, $n = 4$ (*, $p < 0.05$ compared to the corresponding values of WT plants using a two-tailed *t*-test).